CHAPTER IV

DETECTION OF POLYCARBOXYLIC ACIDS FROM SODIUM NITRATE CRYSTALLITES USING INFRARED IRRADIATION

4.1. Motivation

MALDI as an analytical tool has almost exclusively been practiced with ultraviolet lasers, but the potential advantages of IR-MALDI, along with increased availability and cost effectiveness of infrared light sources, has resulted in a growing number of practical and fundamental studies using infrared excitation. Many potentially desirable matrices have vibrational bands in the mid-infrared region, which allow targeting of intrinsic vibrational modes of a system, eliminating the need for addition of a potentially unfriendly matrix. Work with biologically benign compounds like glycerol [1-3], water ice [2,4] – including waters of hydration [5], and polyacrylamide gel [6], in the 3.0 [1,2,5], 6.0 [4,6] and 10.6 μm [3] ranges has shown that these compounds can serve as chromophores for absorbing laser energy and, presumably, as agents for assisting in ion formation. Our motivation for the experiments described in this chapter was to utilize mass spectrometry using intrinsic vibrational excitation as an alternative method for the analysis of mixed hazardous wastes resulting from nuclear fuel processing. In addition to achieving preliminary successes towards this goal using waste simulants, we were also able to shed light on the mechanism of cation formation for light molecules in the presence of sodium ions and to evaluate the relevance of several prevailing models of ion formation in MALDI for this system.

Large quantities of chelants - including EDTA, HEDTA and citric acid, nitrates and nitrites were added to the hazardous waste products now stored in underground tanks. In the evolving tank environment, condensed-phase reactions between these organic chelators (fuel) and nitrate/nitrite salts (oxidizers) could lead to the undesirable release of radionuclides and toxic materials to the environment [7]. As the tank waste ages, chemical and radiolytic degradation of the chelators into smaller compounds reduces the organic fraction available as fuel for these potential reactions. Hence knowledge of the relative abundance of organics in the tank wastes indicates the extent of degradation, and the use of mass spectrometry improves the speed and

accuracy of the risk assessment required prior to waste treatment or relocation. However, the harsh chemical and radioactive environment and presence of large amounts of sodium introduces a number of complications into conventional analyses of the organic content.

Several MALDI studies have already demonstrated the identification of tank waste simulants using conventional matrices [8,9]. We have taken the unique approach of using sodium nitrate, an intrinsic component of the waste composite, as our matrix and tuning our laser to match one of its vibrational absorption modes, eliminating the need for the addition of an exogenous matrix and avoiding potential matrix-analyte chemistry. In previous reports we have described early successes in qualitatively and quantitatively identifying the organic species of interest for addressing the tank waste aging problem, as well as showing that analysis of mixed samples is not likely to be prohibited by the competitive suppression of functionally similar species [10,11].

In the particular case of MALDI-mass spectrometry (MS), alkali ions and cations are often observed even without the addition of salt compounds, due to the ubiquitous presence of sodium and potassium atoms as trace contaminants. Metal ions are sometimes added to compounds containing no acidic or basic groups such as polymers [12] and carbohydrates [13] to increase ion yield. However, alkali atoms are known suppressants of positive ion signals for other classes of compounds both in MALDI [8,14] and for other ion-detecting analytical techniques. Additionally, analytes that form multiple alkali adduct peaks can lead to reduced signal/noise for a defining peak and result in peak broadening for larger molecules, complicating accurate identification [15,16].

The key results of these studies are: (1) that the observed ions are strongly dependent on the specific ablation pathway caused by the thermal and wavelength-dependent optical properties, (2) that they appear to be formed by gas-phase processes, and (3) that the memory of any cation complexes characteristic of the solid state is lost. The data supporting this result include wavelength-dependent mass spectra, especially by observation of sodium adduction patterns, and the dependence of ion species on solution pH. Because of the simple structures of the molecules involved, it is possible to make some reasonable conjectures about the specific binding sites of the sodium ions and the effect of ionization on the structure of the ion complexes observed, and recent computational modeling at least qualitatively confirms observations of the adduction patterns. Importantly, because the initial laser absorption event involves purely

vibrational excitation, these conclusions about the ionization mechanism remove the ambiguities that arise from the possibility of laser-induced photochemistry during ablation with ultraviolet lasers.

4.2. Two models of ion formation. 'Precharged' ions and secondary reactions

Attempts to elucidate the mechanisms of ablation and ion formation in MALDI have been complicated by the wide range of experimental apparatus and material systems practiced in the community. This variety frustrates a collective description of the generic phenomenon, or rather suggests that there is no single model applicable to all systems. While several recent papers have presented models of ion formation in MALDI, we are concerned here particularly with understanding ion formation by alkali cationization, and it seems prudent here to briefly review the prevailing models of ion formation in general and the role of cation formation in particular. Current models of ion formation in MALDI can be generally divided into three groups, representing the distinct temporal stages in the MALDI process when the ions eventually observed may be formed: solution-phase charge associations, 'primary' events resulting directly from laser-material interactions and 'secondary' events, those occurring as a result of chemistry in the selvedge [17]. A discussion of primary processes was included in Section 3.4, and the evidence presented in that chapter showed that several putative processes did not appear to be determinative for the mass spectra obtained from our matrix-analyte system. Following is a summary of the principal tenets and supporting evidence of the models of 'precharged' ions and secondary reactions, as well as their inclusion of cation formation and IR-MALDI events.

4.2.1. Ion formation by 'precharged' species- the cluster ionization model

MALDI as it is practiced today came from efforts to extend the mass range to larger molecules than those observed in matrix-free laser desorption and ionization and secondary ion mass spectrometry, where through various means molecules which already had some charge character were liberated. It thus seemed natural to suspect that similar mechanisms might be active in MALDI, although no substantive framework was developed to support such a model until recently. Development of this idea has largely been due to the work of Karas and collaborators, who posit that charge associations formed by the analyte in the solution state are

roughly retained during crystallization and merely liberated during the ablation event [18,19]. Evidence for this model includes observations of indicator dyes during crystallization [20], controlled acid-base chemistry of selected matrix and analyte pairs [21], and measurements and consideration of initial ion velocities [22]. Indicator dyes were tested with a variety of common matrices at their intrinsic pHs, and the indicators were observed to retain their color upon crystallization, suggesting both that the solution phase charge association was roughly maintained and that residual solvent was incorporated in the crystal, the latter fact which was confirmed separately [20]. The mass spectra of the indicators in all of the tested matrices qualitatively agreed with the predicted charge state, *i.e.*, dyes that were protonated in the solution and condensed phases for a given matrix also appeared in the mass spectra as protonated ions. Likewise, when the dyes were combined with a matrix with an intrinsic pH above the dye's equivalence point, ensuring neutralization or deprotonation, the intensity of the protonated ions either disappeared or was greatly reduced, and only cations were observed. A fundamental assertion of the model is that a critical amount of material is ejected in clusters, some of which may have a net charge either due to mechanical charge separation during the ablation process or cluster photoionization [19], and that subsequent evaporation of neutrals from the charged clusters may result in the appearance of singly charged analytes [18]. As charge reduction and neutralization are likely to be highly efficient, ion formation represents a minority process, and the resulting ions are considered 'lucky survivors' of the ablation event. The identity of the surviving species necessarily is determined by the gas-phase basicities and acidities of the cluster components [21].

Numerical simulations of the MALDI process seem to confirm the importance of clusters in ion formation, showing that the transition from molecular desorption to cluster ejection with increasing laser fluence occurs at fluence values concomitant with experimental values near the threshold of analyte ion formation [23], although the simulations themselves, limited by computational power, do not extend to long enough time scales to fully predict ion formation. Measurements of initial ion velocities have also been adduced in support of the importance of cluster formation [22]. The model suggests that the analyte incorporation into the matrix lattice is necessary, and that both matrix and analyte ion species are formed in the same temporal and spatial regimes. Most measurements of analyte initial ion velocities are independent of mass, charge state, and laser fluence, and rather depend on the matrix used, as well as other preparation

protocols that affect the crystallization process [24]. Although clusters are not generally observed in mass spectra, this is assumed to be a consequence of the low pressures employed in most MALDI apparatus, and both experiments at elevated pressures [25] and tandem MS/MS selection of random 'chemical noise' peaks [26] indicate that abundant [n matrix + analyte]$^+$ clusters are generated during laser ablation.

Since the attachment of alkali atoms does not require the energies necessary for processes involving ionization or proton transfer, some have suggested that alkali cations are formed prior to laser irradiation and liberated by a thermal desorption mechanism, akin to matrix-free LDI [27,28]. An experiment comparing ion species generated by front-side and rear-side ablation found that only cations were observed from rear-side ablation, where no photochemistry was possible, in contrast to both protonated and cationized species from the same sample under front-side ablation conditions, which was interpreted as supporting a thermal desorption mechanism for cations [29]. In the cluster ionization model, cations are but one end product of evaporating clusters. However, cation formation is unlikely to compete favorably with protonation for many analyte:matrix combinations, and a general framework predicting the surviving species in the cluster ionization model has not been published. The model does distinguish between cations liberated during cluster evaporation and those created by gas-phase chemistry. A recent analysis of initial ion velocities of analytes with basic functional groups shows that both protonated and cationized species possess similar initial high ion velocities, suggesting that both species are originally incorporated in the matrix and liberated through a soft desorption process [22]. However, small neutral molecules, such as oligosaccharides, are observed as cations with significantly lower initial velocities, suggesting that for these molecules thermal desorption precedes gas-phase cationization processes [22].

Since this cluster model does not require matrix photoionization, but only cluster generation, the inclusion of IR-MALDI is straightforward. However, the longer penetration depths for the laser wavelengths and matrices used in IR-MALDI is known to result in larger volumes of ablated material compared to UV-MALDI [30,31], suggesting that larger clusters are ejected than in UV-MALDI. The potential differences caused by larger clusters has not been discussed in the context of IR-MALDI, but a recent measurement of initial velocities and the 'virtual desorption time' argues that large clusters can not explain the ions observed in MALDI [32]. However, the ejecta from matrices under IR-MALDI conditions have not been well

characterized, so the assumption that primarily larger clusters are removed is not known, and certainly does not necessarily contradict the results of this experiment. Furthermore, since only a minority fraction of the ablated material are observed as ions, then even if IR-MALDI results primarily in the ejection of large clusters, then a small fraction of molecular species could still account for the observed ions.

4.2.2. Ion formation by secondary plume processes

While cluster-based models appear to address some of the general phenomena in MALDI, they have yet to establish the theoretical basis that exists for models based on secondary processes [33-35], meaning those processes occurring after irradiation in the expanding plume, or selvedge. This model acknowledges that many different ion species are likely to be formed during the irradiation event, depending on the irradiation parameters and materials used, but suggests that the final ion species are determined by the thermodynamic properties of the ejecta provided that several conditions are met. This model requires: (1) good mixing of matrix and analyte in the sample, (2) sufficient collisions in the plume and (3) thermally accessible activation energies at typical plume temperatures. All three conditions are related to the need for a sufficient number of collisions in the selvedge for charge transfer to happen in thermodynamic equilibrium. Evidence for the cardinal role of secondary reactions is provided by the analysis of matrix and analyte species with known gas-phase properties. For example, it has been demonstrated that if the matrix ionization potential is greater than that of the analyte, then electron transfer to the analyte is favored and the radical ion is observed, while the use of a matrix with a lower ionization potential fails to lead to analyte radical ions [36]. Likewise, a mixture of peptides with different proton affinities will yield spectra of both compounds at laser fluences just above threshold, but at elevated laser fluences, and presumably denser plumes, an equilibrium situation is obtained and only the peptide with the higher proton affinity (PA) is observed [34]. This phenomenon, termed the analyte suppression effect, is related to the matrix suppression effect, where for particular analyte:matrix ratios, only analyte ions are observed [37-39]. Matrix suppression has been observed for a wide number of analyte and matrix combinations, and for systems where the respective PAs are known, the analyte PA is greater than the matrix PA and the analyte serves as the limiting reactant – if the analyte is present in

sufficient concentration, little or no matrix ions are observed. Ion formation by secondary processes offers a ready explanation for the observations presented in Chapter 3 of similar spectra over a wide range of photon energies and fluxes. Regardless of the variety of primary ions created during irradiation, these ions are converted by secondary plume reactions to the same thermodynamically favored ions. This model seems fully compatible with IR-MALDI, as any memory of different initial ion species is not retained.

Both theoretical and experimental models have been developed to explain cation formation by gas-phase processes [17,35,40,41]. In one study, Belov *et.al.* showed in a crossed beam experiment that delayed laser-generated Na^+ ions from a second target, when intercepting the plume from a matrix–peptide sample at a sub-ion threshold fluence, generated similar, cationized species as those observed with only the primary desorption beam at above-threshold fluences [40]. Recent measurements of gas phase sodium affinities for MALDI matrices [42-44] have made it possible to confirm the products of various matrix:analyte combinations based on thermodynamic considerations. Further, this model makes it possible to address the question as to why cation adducts are observed at all, given that proton affinities are always significantly higher. If the analyte proton affinities are less than matrix proton affinities, then the matrix abstracts the protons and analyte cationization becomes the ionization route of last resort [35]. Studies involving divalent transition metals as cationizing agents seem dependent on the

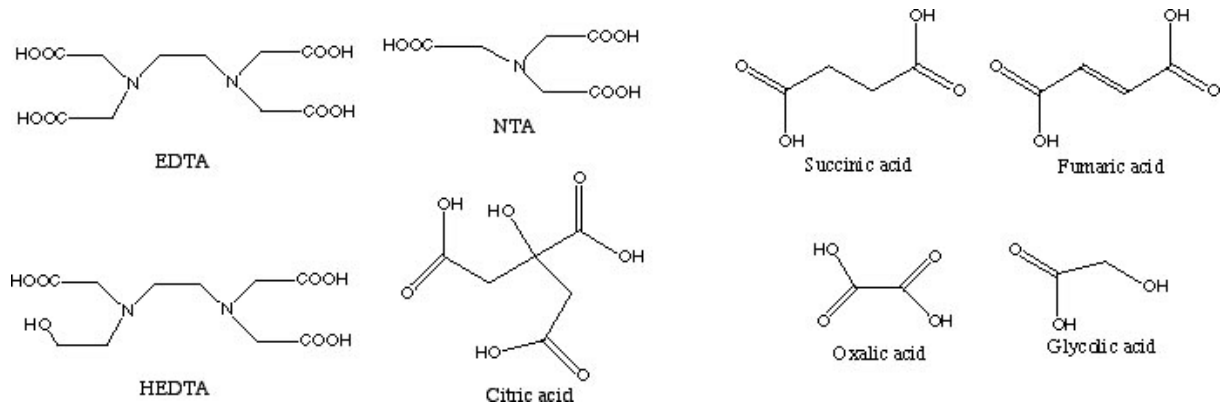

Figure 4.1. The polycarboxylic compounds studied included both chelators (left) and several of their degradation products (right).

particular system studied, presenting evidence for ion formation in both the gas [45] and condensed phases [46,47].

4.3. Experimental results

4.3.1. Ion species as a function of wavelength

The compounds used in this study, described more fully in Sec. 2.4 and shown in Figure 4.1, were selected from a recipe for tank waste simulant in the literature [48]. They include the larger chelating compounds originally added to the waste as well as several of their principal degradation products. All spectra taken of the polycarboxylic acids in sodium nitrate at the nitrate stretching mode near 7.1 μm were dominated by peaks due to the sodium nitrate matrix, especially those belonging to Na^+ and $[Na + NaNO_3]^+$ ions. Figure 4.2 shows a mass spectrum of succinic acid in $NaNO_3$ at a 1:50 molar ratio, showing both a) the original spectrum, displaying typical intensities of $NaNO_3$ peaks compared to carboxylic compound peaks, indicated with an asterisk, and b) the same data with the $NaNO_3$ peaks erased. The major peaks in Figure 4.2(a) are listed in Table 4.1. The peaks highlighted in Figure 4.2(b) represent sodium adducts of the parent molecule, a sodium nitrate-succinic acid complex, and a succinic salt dimer. All compounds added to the waste simulant possess several carboxyl groups and gave

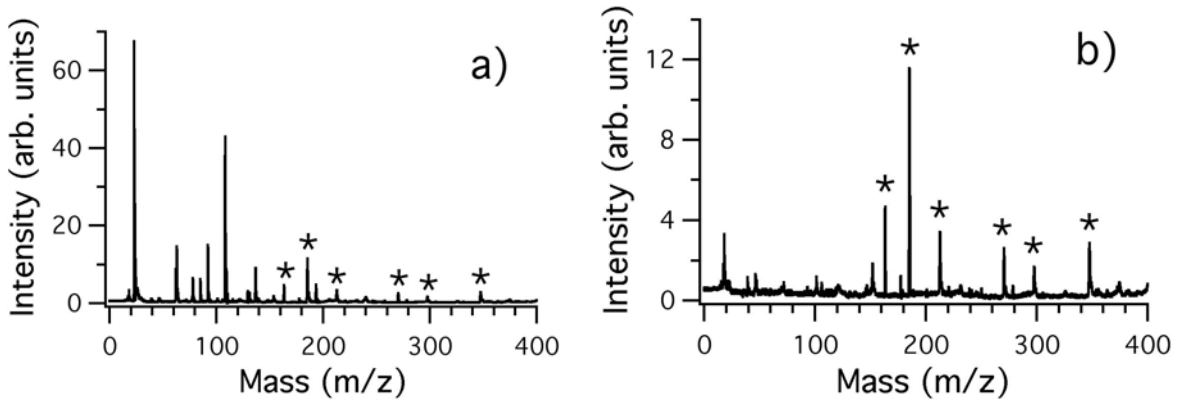

Figure 4.2. a) Positive ion spectrum of succinic acid in $NaNO_3$ at a 1:50 molar ratio. The succinic cation peaks are marked with asterisks. b) The same spectrum as in a) with the major $NaNO_3$ peaks removed. Note the vertical scale difference for the two spectra. The peaks are identified in Table 4.1.

Table 4.1. Peak identification for the spectra of succinic acid shown in Figures 2(a) and 3(a).

$NaNO_3$ (+) ions		Succinic acid (+) ions		$NaNO_3$ (-) ions		Succinic acid (-) ions	
Na	23	S + 2Na - H	163	NO_3	62	S - H	117
Na_2OH	63	S + 3Na -2H	185	$Na(NO_2)_2$	115	(unknown)	145
Na_2O	78	(unknown)	214	$M(NO_2)$	131	M + S – H	202
Na_3O	85	M + S+ 3Na – 2H	270	$M(NO_3)$	147	M + S + Na – 2H	224
Na_2NO_2	92	(unknown) + M	299	$M_2(NO_2)$	216	2M + S + Na–2H	309
Na_2NO_3	108	2S + 5Na – 4H	347	$M_2(NO_3)$	232		
$Na_2(NO_2)_2$	138						
NaM_2	193						

S = Succinic acid, M = $NaNO_3$

similar fingerprint patterns of salt peaks. Aside from a few fragment peaks of the larger compounds and clusters containing $NaNO_3$, the observed polycarboxylic ions were primarily of the series $[A + n\text{Na} - (n\text{-}1)\text{H}]^+$, where A denotes the polycarboxylic compound and $n = 1$ to $m + 1$, where m = the number of carboxyl and hydroxyl groups. Only singly charged ions were observed in these studies.

Negative ion spectra were investigated both to provide a complementary means of speciation and to address mechanistic questions of ion formation. The acidic character of the carboxyl group suggests that they are more likely to be observed as deprotonated negative ions than positive ions. A study of similar compounds using 2,5-DHB as a matrix found that the smaller acids, such as succinic acid, indeed displayed stronger signals in negative ion mode, while chelating compounds with basic amine groups (EDTA, HEDTA) appeared more strongly

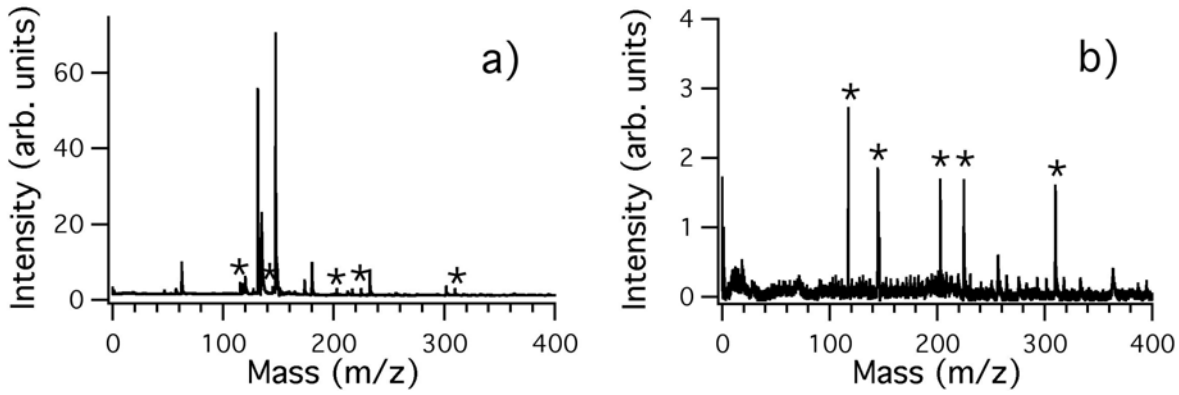

Figure 4.3. a) Negative ion spectrum of succinic acid in $NaNO_3$ at a 1:20 molar ratio. The succinic ion peaks are marked with asterisks. b) The same spectrum as in a) with the major $NaNO_3$ matrix peaks removed. Note the vertical scale difference for the two spectra. The peaks are identified in Table 4.1

in the positive ion mode [8]. In our study, however, negative ion peaks associated with the polycarboxylic acids could only be obtained for a few of the compounds and only at greater analyte-to-matrix ratios than necessary for positive ions, reflecting the efficiency of salt formation. Figure 4.3 shows a negative ion spectrum of succinic acid in $NaNO_3$ at a 1:20 molar ratio, showing both a) the original spectrum and b) one with the matrix peaks removed. A listing and partial identification of the ions is given in Table 4.1. The deprotonated anion is observed, but anions of the succinic salts are not strongly expressed, especially in comparison to the preference for highly salted species in the positive spectra, in keeping with general observations in a conventional MALDI experiment [49]. Clusters of matrix and succinic appear both with and without a sodium atom. Sodium atoms are widely known to assist in cluster formation of conventional matrices, but there seems not to be a significant enhancement for this data.

While the nitrate-stretching mode near 7.1 μm is clearly the strongest absorption feature for sodium nitrate, we also irradiated our sample at other wavelengths for additional or complementary information. In our attempt to understand the mass spectra acquired at various irradiation wavelengths, we were careful to observe that the absorption profile of the sample is potentially different from the absorption spectrum one might find in a standard library reference, where the matrix is measured in an IR transparent pellet or mull. In Figure 4.4 we compare the absorption spectrum of $NaNO_3$ both a) in a KBr pellet and b) in a standard sample preparation, as measured by ATR FTIR (Section 2.4). We see that in the sample preparation [Fig. 4.4(b)]

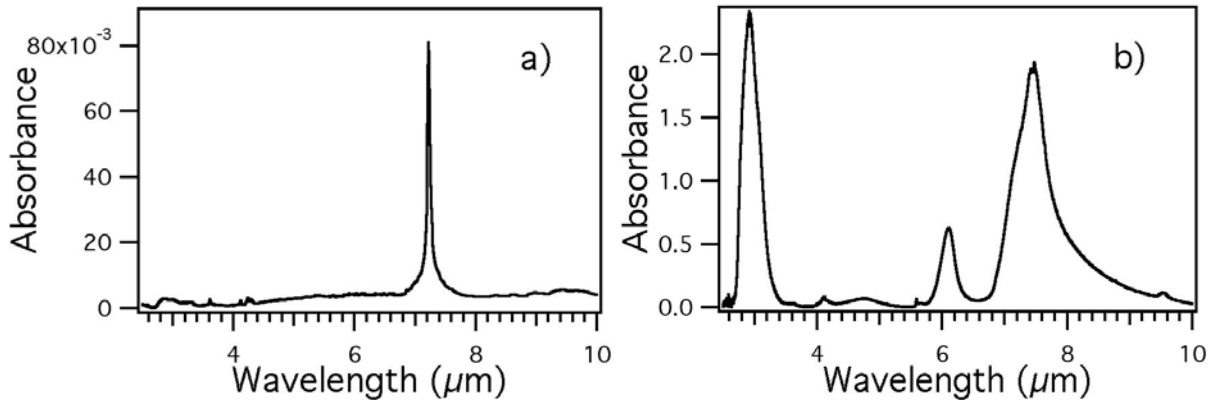

Figure 4.4. FTIR absorption spectrum of $NaNO_3$ a) in transmission through a KBr disk and b) in attenuated total reflectance (ATR) from a sample as used in our experiments. Significant band broadening, as well as additional peaks, due to water incorporated during crystallization are evident in the ATR spectrum.

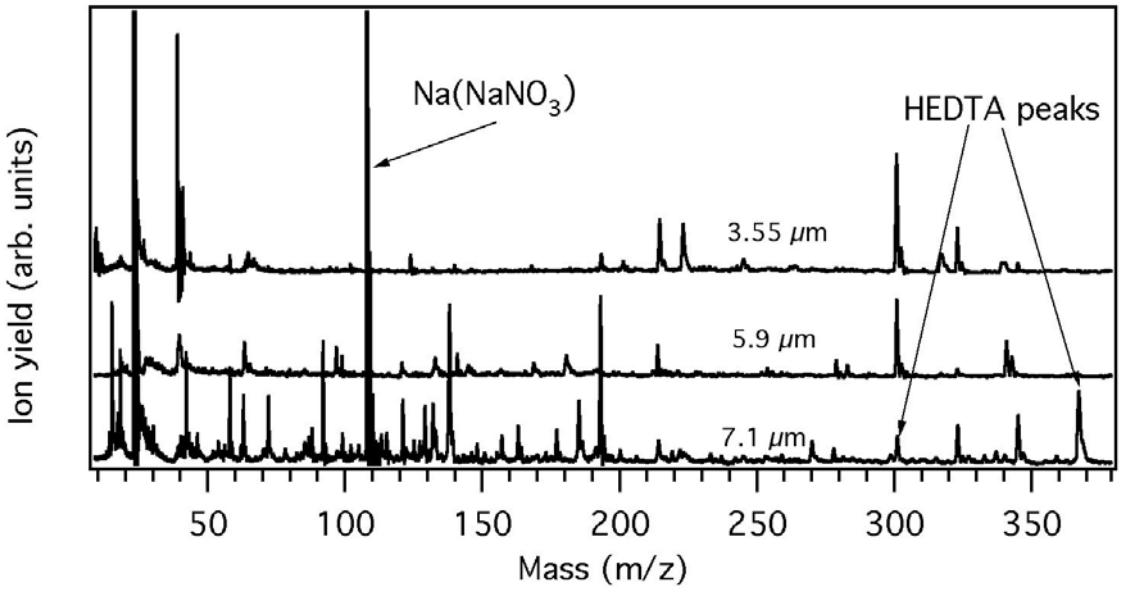

Figure 4.5. Mass spectra obtained with irradiation wavelengths of 7.1, 2.9, and 3.55 μm. Note that the matrix peaks consistently present at 7.1 μm are largely missing at the other wavelengths, and that the degree of sodiation of HEDTA shifts significantly to fewer adducts.

residual water is trapped in the microcrystallites, even after extended drying, resulting in new peaks and considerable broadening of the nitrate stretching mode at 7.1 μm.

Several wavelengths other than the nitrate-stretching mode were found to be useful at generating ions of tank waste compounds; water modes at 2.9 and 5.9 μm, and the nitrate overtone mode at 3.55 μm. These other wavelengths were generally less reliable at producing useful ion signals on a shot-to-shot basis, and in each case, the mass spectra displayed significant differences with respect to mass spectra produced at 7.1 μm [Figure 4.5]. Most notably, the matrix peaks that dominate the mass spectra at 7.1 μm [see Figure 4.2 and Table 4.1] are not present, or are only weakly present, at the other wavelengths. In addition, the degree of sodium adduction is much less pronounced. For example, studies of HEDTA at 7.1 μm showed that the ion with four sodium atoms had the highest intensity, while for these other wavelengths the ion with only one sodium atom dominated the spectrum. This trend towards lower sodium number was observed for other compounds as well. All attempts to generate positive carboxylic ions at wavelengths that did not correspond to an absorption mode were unsuccessful at the available laser energies.

A clue to the differences in the mass spectra can be found in the comparison of the absorption profiles at the different wavelengths. The IR absorption coefficient of sodium nitrate

in KBr was found to have a molar decadic coefficient of 3300 L/(mol*cm) at the nitrate stretching mode, corresponding to a 1/e penetration depth of about 70 nm, while the penetration depth at the 3.55 μm overtone was measured to be 8 μm. At 2.9 and 5.9 μm, the absorption is likely due to residual water trapped during crystallization, with a possible smaller contribution by the carboxylic ligands of the added compounds at 5.9 μm. These facts make any determination of laser penetration depths at these wavelengths subject to a specific sample and temporally dependent, and certainly not possible with a qualitative measurement like ATR FTIR. However, the mass spectra near the water modes resemble those obtained at the overtone mode both with respect to the general absence of sodium nitrate ions, the reproducibility of the spectra on a shot-to-shot basis and the patterns of sodium adduction.

The penetration depth measured for the nitrate mode at 7.1 μm, which generated the most reproducible mass spectra, is closer in value to those found for the matrices and wavelengths used in UV-MALDI (10s of nanometers) [30,50] than those successfully used in IR-MALDI (10s of microns). For example, the penetration depths for the OH and CH absorption modes most commonly targeted for a common IR matrix, succinic acid, were measured to be between 20-40 μm [30]. This leads to considerably more material removed per laser shot, which can affect shot-to-shot reproducibility. For 'dried droplet' preparations of typical IR matrices, often the sample is consumed after 2-5 laser shots on the same spot when the laser intensity is near the ion threshold. In contrast, several hundred laser shots can often be obtained from the same spot under UV-MALDI conditions, as well as from our sodium nitrate samples.

The significant differences in penetration depths at the tested wavelengths point to different mechanisms of material removal. (A more complete discussion of the effect of physical properties on ablation is given in Chapter 5.) Irradiation at the nitrate stretching mode, with the short penetration depth (70 nm), results in a high density of vibrational excitation, leading to high heating rates and efficient bond breaking, and presumably reduces the sample into small clusters and molecular and fragment species. The high temperatures and kinetic energies in the evolving plume will result in a high collisional cross section, resulting in the separation of ion pairs and abundant sodium ions. This is reflected in the mass spectra (see Figure 4.1 and Table 4.1), where the major species are sodium ions and fragments of sodium nitrate. However, the longer penetration depth (8 μm) at 3.55 μm places the system in a state of moderate confinement, where ablation proceeds by the ejection of larger clusters. This causes less

efficient charge separation and sample disintegration, resulting in fewer gas-phase sodium ions. The mass spectrum of a sample irradiated at 3.55 μm in Figure 4.5 accordingly shows less sodium and small ions, and the degree of adduction for HEDTA is likewise reduced. The latter

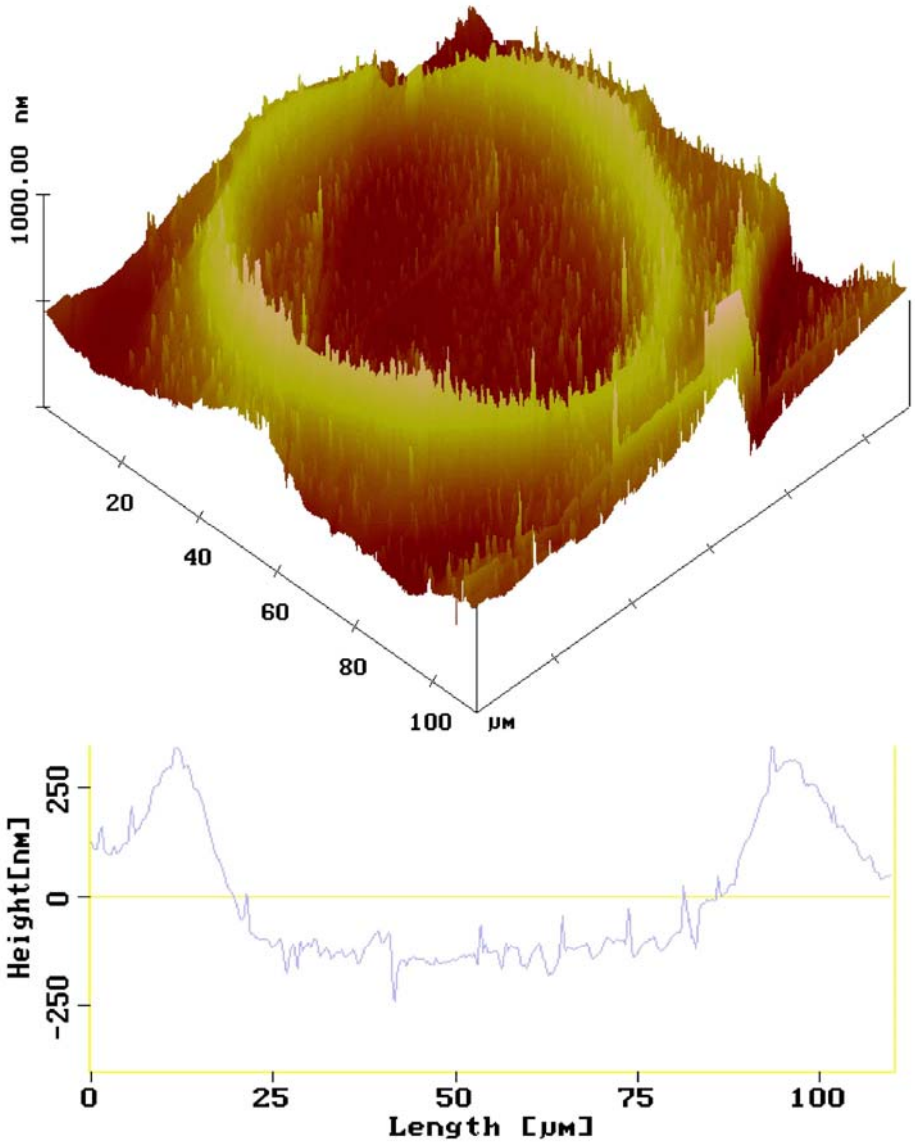

Figure 4.6. AFM image of the surface of a single $NaNO_3$ crystal irradiated by a single laser shot at an irradiance just above the threshold for ion generation, viewed both from above and in cross section. Approximately 75% of the crater is redeposited around the rim of the crater. Cracks in the bottom of the crater (not easily seen here) give evidence for refreezing of molten material.

fact is somewhat surprising, for if salt formation occurs during crystallization, then the salt should still be observed in the mass spectra. This implies either (1) that the violence of the ablation process removes the sodium atoms, which are then replaced by protons, (2) only the acids, and not the salts are energetically able to form stable ions, or (3) we are observing species that are not representative of the sample, for instance surface molecules or molecules from the boundaries of fracture sites. We must remember again that the ion yield represents a small fraction of the total material ablated, even more so at 3.55 μm, with the assumed larger amount of material removed without a corresponding increase in ion yield. A discussion of the ablation processes intiated by exciting residual water in the sample is more complicated because of the inability to quantify the absorption coefficient and the importance of the mode of excitation. In summary, these results strongly support the picture of cation formation by gas-phase processes.

Figure 4.6 shows a scan of a single laser shot on a sodium nitrate single crystal imaged by atomic force microscopy (AFM) (Nanoscope III, Digital Instruments, Santa Barbara, CA), showing a crater with a rim of material around the periphery. The laser beam spot size at the surface was measured by thermally sensitive paper to be elliptical with major and minor axes of 180 μm and 150 μm, respectively, while this image shows an elliptical impact area with axes of 80 and 70 μm, respectively, reflecting the Gaussian nature of the beam and energy threshold for modification. The laser energy used here was 250 μJ in a 250 ns pulse, just above the threshold for ion generation. Analysis of the crater and surrounding area shows that the height from the crater bottom to rim was about 390 nm, but that the distance from the rim to surface outside of the crater was about 320 nm. Much of the material from the crater is redistributed radially outward from the center and accumulates around the margin of the affected area. Additionally, we see that cracks are formed in the crater bottom due to stresses formed during the refreezing of molten material. These results are consistent with resonant laser irradiation of calcium carbonate [51], a compound that is isoelectronic with sodium nitrate and belongs to the same crystal group, in showing planar material removal from the bottom of the crater.

Optical microscopy of damage to single crystals irradiated at 3.55 and 5.9 μm at fluences just above ion threshold reveals point-like craters suggesting defect-initiated ablation. Profilometry of laser damage at these wavelengths was not possible as the extent of the damage was beyond the range of the AFM, but partial scans confirmed the violent nature of the injury. Observation showed fracture along cleavage planes and removal of large chunks near the center

of the affected area, revealing the Gaussian beam profile and consistent with damage due to explosive sub-surface boiling and absorption by impurities and defects [51,52]. Hence, despite the greater yield of removed material, the material is in the form of platelets or large chunks, and reduction to molecular species, and presumably ions, should be less efficient.

The threshold energies for ion generation varied depending on sample preparation and wavelength. For a multicrystalline sample, such as typically used in our experiments, the threshold was ~70 μJ in a 100 ns pulse, much lower than that necessary for surface modification and ion generation from single crystals. This is expected due to the greater surface area and defects present for these samples. Laser damage to and ion generation from single crystals using 3.55 and 5.9 μm irradiation was accomplished only with laser fluences an order of magnitude higher than at 7.1 μm, or ~20 J/cm^2. For most laser shots, in fact, no surface modification (or ion generation) was observed. This is not so surprising at 5.9 μm, since the water content of the single crystals is likely to be much lower than that present in the defective multicrystalline samples.

4.3.2. Sodium adduction as a function of structure

Given that the polycarboxylic acids are surrounded by a high molar excess of sodium ions, it is not surprising that we see these compounds appear in the mass spectra possessing multiple sodium atoms; both neutral atoms participating in salt exchange and ions. This section reports on the degree of sodium adduction (both salt formation and cation attachment) for the compounds in this study. While the multiple peaks more than suffice for identification, we closely examined their patterns to understand the energetics and conformations prevalent for this class of molecules. The studies in this section were accomplished for individual compounds in sodium nitrate at molar concentrations less than 1:30. Protonated ions were observed only for HEDTA at these concentrations, but could be observed for some other compounds at higher concentrations.

The compounds considered first are those shown in Figure 4.1 that do not possess amine centers. We find that the number of sodium atoms associated with these compounds ranges from 1 to n+1, where n equals the total number of functional groups. For oxalic and succinic acids, compounds with two carboxyl groups, the most prominent peak represents the compound with

three sodium atoms, which can be described as $[A + 2Na - 2H]Na^+$, where A represents the polycarboxylic acid (see *e.g.*, succinic acid in Figure 4.2 and Table 4.1). The simplicity of the compounds' structures suggests that both carboxyl groups become salted, and that an additional sodium ion is chelated by one (or both) of the salted carboxyl groups. Both compounds also expressed ions with two sodium atoms, which could be described either as a protonated disodium salt, $[A + 2Na - 2H]H^+$, or as a sodiated monosodium salt, $[A + Na - H]Na^+$, though the discussion below suggests the latter. Oxalic acid, but not succinic acid, yields ion peaks with one sodium atom, $[A]Na^+$ (or $[A + Na - H]H^+$). For these compounds, the most intense ion contains the maximum allowed number (3) of sodium atoms, *i.e.*, two sodium atoms that participate in salt formation, and one sodium ion that binds to the molecule. The normalized ratios of the adduct distributions for all studied compounds is shown in Figure 4.7.

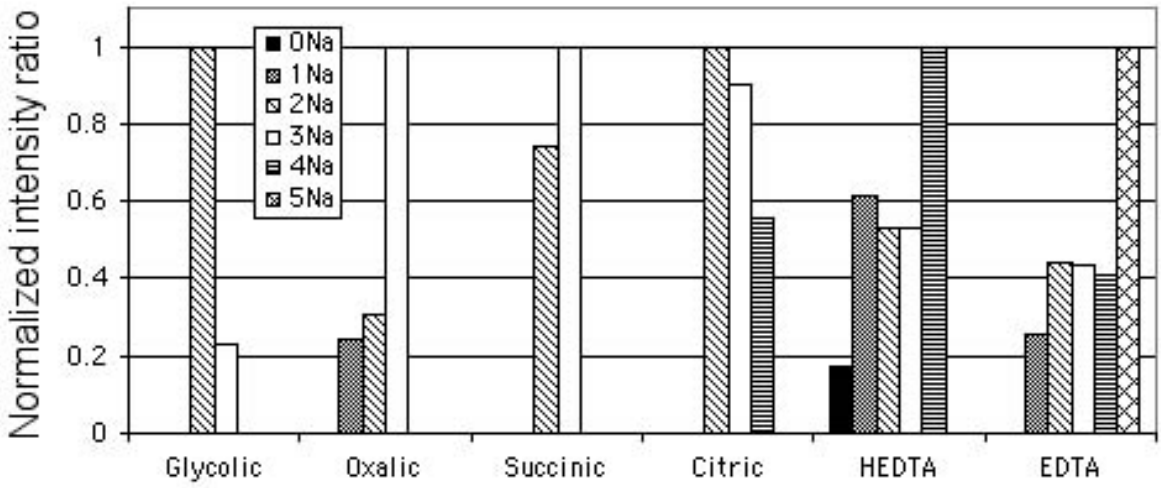

Figure 4.7. The relative intensities of the positive ions peaks containing different numbers of sodium atoms. While most of the compounds show higher intensity peaks for the highest number of sodium atoms, glycolic and citric acids show a decrease. The peak intensities were first normalized to matrix peaks and then scaled so that the most intense peak had a value of unity.

Glycolic acid, with one carboxylic group and one hydroxyl group, shows significant peaks for only $[A + 2Na - 2H]Na^+$ and $[A + Na - H]Na^+$, with the less substituted ion present at a higher intensity. Based on the observations for oxalic acid, the glycolic acid cation with three sodium atoms likely has two sodium atoms associated with the carboxyl group and one with the hydroxyl group, with the positive charge residing on the carboxyl group. Citric acid, with three carboxylic and one hydroxyl groups, does not follow the pattern in showing one more sodium

than the number of functional groups. Instead, the most substituted ion observed contains four sodium atoms, while the most intense ion possesses only two sodium atoms [Figure 4.7].

A comparison of the amine based chelating compounds studied in this work shows similar behavior to that observed for succinic and oxalic acids. All three compounds, NTA, HEDTA, and EDTA possess several acetic acid groups; HEDTA also possesses a hydroxyl group. The amine center is well known to participate strongly in the chelation of transition metal ions, and less so for sodium atoms, either directly to the nitrogen atom or coordinated by both the nitrogen atom and (a) carboxyl group(s). However, despite these likely additional arrangements, the generic pattern seems similar to that seen with the polycarboxylic acids lacking amine centers. All compounds yielded multiple adduct ion peaks, and for each compound the maximum number of sodium ions observed was one greater than the number of carboxyl groups (Figure 4.7, data for NTA not shown). This suggests that the less acidic proton on the hydroxyl group of HEDTA does not participate in ion formation, in keeping with the observation for citric acid but contrary to that for glycolic acid. HEDTA was the only compound for which significant intensities of protonated peaks appeared.

Metal-ligand complexes are important in many disciplines, including biological processes [53] such as cation transport through membranes [54,55], interface physics [56], and mass spectrometric systems [42-44], and recent experimental and computational advances have improved our understanding of their energetics and conformations for a variety of ligands [42-44]. Unfortunately, the sodium binding affinities of the molecules studied here or the steric effects of the association of a sodium ion to a salted carboxyl group have not been documented in the literature. However, computational work in our group has returned preliminary values for sodium binding affinities for several of these compounds and is presented below. Computational studies of other simple structures with carboxyl groups have shown that electrostatic attraction occurs between the sodium ion and the dipole moment of the carboxyl group and, to a lesser extent, ion induced dipole moments with the molecule [43,54,56]. However, molecules with additional functional groups often had more favorable multidentate conformations for Na^+-carboxyl associations. These include chelation of the carbonyl oxygen with: 1) a hydroxyl oxygen [42,43], 2) an amino group [43,54,57,58], 3) a second carbonyl oxygen [54,59] or 4) both a second carbonyl oxygen and an amino group [59] - all potential arrangements for our compounds. Sodium affinities for carboxyl-containing MALDI matrices have been measured

and calculated to be about 35-40 kcal/mol (1.5-1.7 eV), much less than proton affinities for the same compounds, which range from 870-910 kcal/mol (9.0-9.3 eV) [42]. This difference in binding energies for hydrogen and sodium extends to most molecules, reflecting the proton's smaller atomic radius, which allows for a stronger electrostatic interaction. The difference in binding strength with atomic radius also suggests that the dipole moment of a salted carboxyl group is stronger than an unsalted one, since the sodium atom will affect a less efficient charge separation with the carboxyl oxygen than the hydrogen atom would. This would result in higher sodium affinities than those mentioned above. However, this putative advantage may be negated by undesirable steric hindrances. Additional experimental data or computational modeling will be necessary to address these possibilities.

Recent calculations of sodium binding affinities for glycolic, oxalic, and succinic acids has been performed (Section 2.6) for the acid, monosodium salt and disodium salt structures and the results are summarized in Table 4.2. While these results will require further refinements, they do agree fairly well for the binding affinities to carboxylic acids listed above. In agreement with the data, we find that for each compound the ion form of the disodium salt is lower in energy that the monosodium salt, which is in turn lower in energy than the acid form. This

Table 4.2 Gas-phase binding energies of several carboxylic acids and salts

Sodium cation of:	ΔG (kcal/mol)
Glycolic acid	- 31
Glycolic acid monosodium salt	-45
Glycolic acid disodium salt	-58
Oxalic acid	-28
Oxalic acid monosodium salt	-41
Oxalic acid disodium salt	-50
Succinic acid	-35
Succinic acid monosodium salt	-48
Succinic acid disodium salt	-61

suggest that the ion formation is governed by the compounds' gas-phase thermodynamic properties, at least when irradiated at the nitrate stretching mode. The primary difference between the oxalic acid and succinic acid results is that the oxalic acid appeared as a cation of the acid, while succinic acid appeared only as the cation of either the monosodium or disodium salt. This may be explained by the stronger binding energies of the succinic acid compared to oxalic acid. Geometrical optimization shows that the most favorable structure occurs from a rotation about the C2–C3 bond, resulting in a ring structure with the sodium ion in a bidentate arrangement with oxygens from both carboxyl groups. Also, we find that the binding energies of glycolic acid follow a similar pattern, but deprotonation of the hydroxyl hydrogen likely results in too high an energy barrier for salt formation to be favored.

Based on these observations, we might expect citric acid, with three carboxylic and one hydroxyl groups, to yield ions with up to five sodium atoms, with the peak having four atoms having the highest intensity. However, the most intense peaks are those with two and three sodium atoms, with a weaker four-sodium peak and no one or five sodium peaks. We presently are not able to rationalize these results based on structural considerations.

The remaining compounds studied are the chelants HEDTA, EDTA, and NTA, which are known to coordinate transition metals through the cooperation of both nitrogen and oxygen atoms. However, the observed spectra show behavior similar to succinic and oxalic acids, suggesting that the ion attachment occurs on the carboxyl group without any additional stability contributed by the amine center. HEDTA, with a hydroxyl group, provides another point of comparison with EDTA and NTA. It does not appear that the ligand participates in salt formation, but may contribute to the overall stability of the ion, given the higher yield compared to EDTA [Section 4.3.3].

4.3.3. The effect of structure on ion intensity

Over the course of these studies, the intensity of the ion yield varied among the polycarboxylic compounds. Due to difficulties in finding universal initial conditions, no systematic evaluation was completed quantifying the response, but observations indicate the compounds generated ion signals according the following qualitative relationship:

Succinic acid > oxalic acid ≈ glycolic acid ≈ HEDTA > citric acid > EDTA

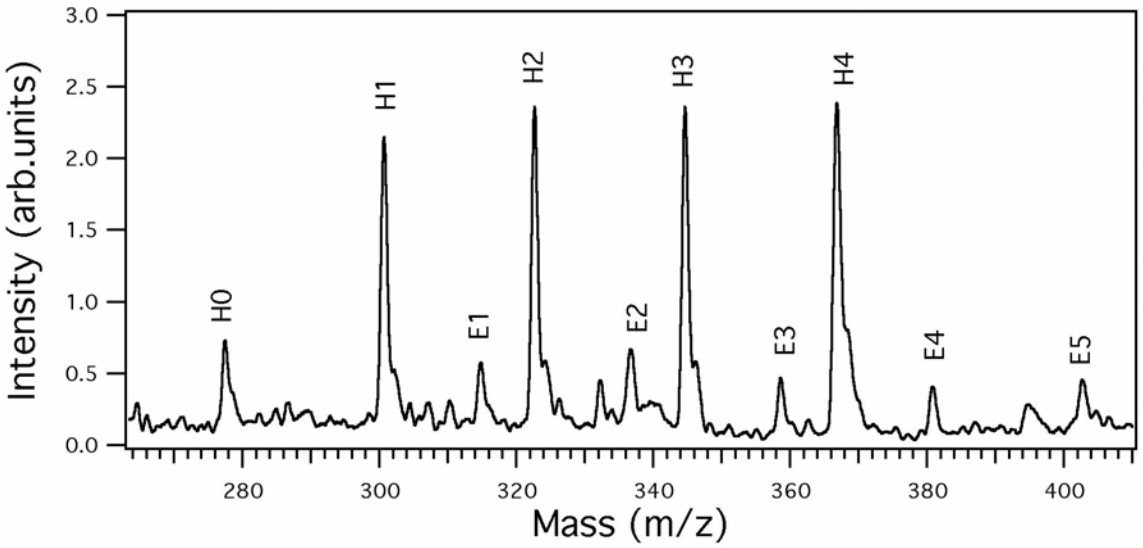

Figure 4.8. Positive ion mass spectrum of equimolar concentration of HEDTA (H) and EDTA (E) in sodium nitrate (each at a 1:86 molar ratio) irradiated at 7.1 μm. The numbers on the peak labels refer to the number of sodium atoms present per compound. Note that for this data set the sodium adduction patterns are somewhat different than the usual distribution shown in Figure 4.7.

One especially noteworthy comparison involves EDTA and HEDTA, which differ only by a substitution of acetyl ligand for a hydroxyethyl group. It was observed that for equimolar concentrations of HEDTA and EDTA, the ion peak intensity from HEDTA is about 5 times greater than for EDTA, as seen in Figure 4.8. (This effect is not caused by competition between the two species as the yield discrepancy is observed for individual preparations.) Since the sodium ion is located on a carboxyl group, then statistically one might expect that EDTA, with one more carboxyl group, would produce a higher yield. One possibility is that while the hydroxyethyl group does not undergo salt exchange (or ion attachment), it may help stabilize a charge-carrying carboxyl group, improving the survival probability of the charged molecule from collisional neutralization. Again, values for the sodium affinities for these molecules may shed light on the difference in ion yield for these two compounds.

4.3.4. Effect of initial solution pH on ion species

An understanding of the effect of solution sample pH prior to crystallization is of importance for both practical and fundamental reasons. Understanding the influence of the sample pH is important for designing analysis protocols for heterogeneous mixtures, particularly in the case of the tank waste composite that motivated this study, where wide variations in pH

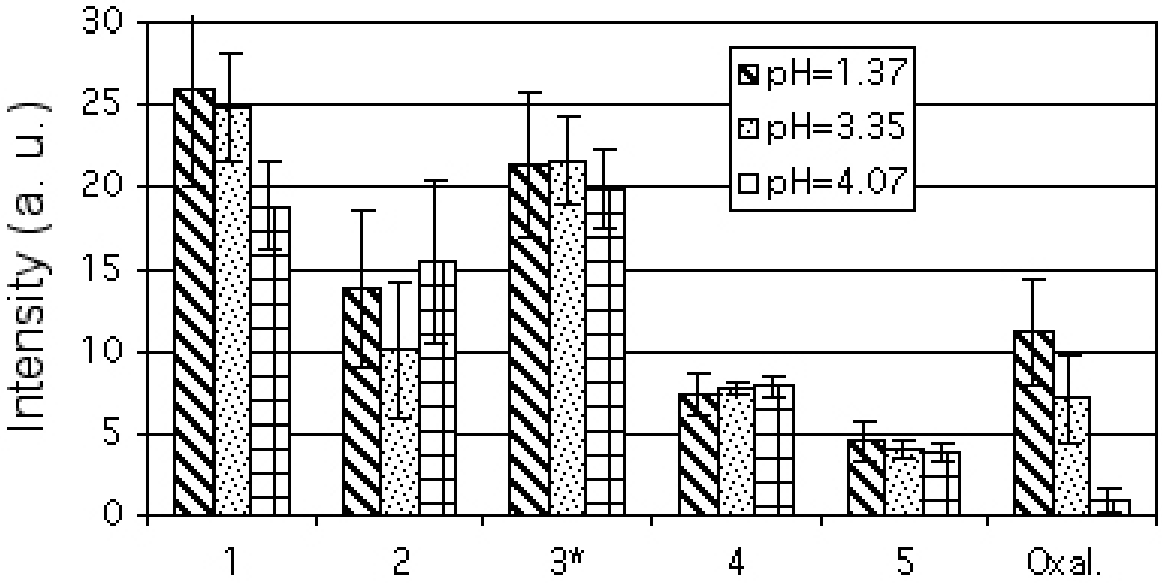

Figure 4.9. The peak intensities of $NaNO_3$ matrix peaks and the oxalic acid (O) $(O + 3Na - 2H)^+$ peak as a function of pH. The data sets 1 through 5 refer, respectively, to the matrix peaks Na_2OH, Na_2NO_2, $Na(NaNO_3)$, $Na_2(NO_2)_2$ and $Na(NaNO_3)_2$. The intensity of the $Na(NaNO_3)$ peak (number 3) was divided by two for display purposes. Oxalic acid ions are clearly sensitive to the initial pH of the sample, showing no signal (for the given concentration) for pH values greater that 4.1.

are known to occur. Additionally, the solution pH also determines the charge associations formed prior to crystallization and ablation, and allows us to evaluate the contribution of preformed ions in the MALDI process.

Our studies varying the initial solution pH found a compound dependent effect on the appearance of ions in the mass spectra. Oxalic acid ions proved quite sensitive to the initial pH. A 1:42 molar ratio of oxalic acid:$NaNO_3$ was prepared, and samples were deposited as the pH was varied to values of 1.4, 3.4, 4.1 and 8.1. For comparison, the equivalence points of oxalic acid are listed in Table 4.2. The intensities of several major matrix peaks were measured to establish a baseline behavior to determine if the matrix peaks were sensitive to the initial pH. Figure 4.9 shows the intensities of both matrix and oxalic acid peaks for the different pH values. While the matrix peaks are relatively insensitive to the initial pH up to pH =8.1 (data not shown for the last point), the intensity of the $[oxalic + 2Na - 2H]Na^+$ peak clearly decreases with increasing pH to a value of 4.1, and no oxalic peaks were detected for a pH value of 8.1. The behavior of the $[oxalic + Na - H]Na^+$ ion displayed a similar dependence on increasing pH (not shown), but the intensity of this peak was quite weak for all but the lowest pH value, not

Table 4.2. Experimentally determined equivalence points (EP) for carboxylic acids in sodium nitrate at concentrations representing sample conditions.

	EP 1	EP 2	EP 3
Oxalic acid	2.55	7.86	
HEDTA	3.80	7.17	10.46
Glycolic acid	7.95		

permitting a comparison of the ratios of the two ions below and above the equivalence point. For this analysis, seven spectra were taken for each pH value, where each spectrum was an average of 10 shots from 10 different spots on the surface.

However, a different behavior was observed in a study of an equimolar mixture of HEDTA and glycolic acid, each at a 1:26 molar ratio to $NaNO_3$. The initial pH values, ranging from 1.8 to 10.2, almost completely span the equivalence points of both glycolic acid and HEDTA shown in Table 4.2. Similar to the results shown in Figure 4.9, the sodium nitrate peaks were found to be insensitive to the initial solution pH. The data shown in Figure 4.10 represent ratios of analyte peaks to $Na_2NO_2^+$, which normalizes the spectra against fluctuations due to variations in surface morphology, laser energy, etc, and similar results were found when using other matrix peaks as standards. The peak intensity of the four adduct peaks was monitored, and with the exception of the HEDTA molecule with one sodium atom, the HEDTA adducts and glycolic acid show no strong dependence on pH. In another study varying pH of a mixture including succinic acid, neither the succinic acid adduct ions or a succinic acid-$NaNO_3$ complex showed any intensity dependence on pH over tested range (data not shown).

Most MALDI samples are crystallized from a solution containing both matrix and analyte species, and the solution ion species are determined by the initial pH. There is generally a consensus in the MALDI community that the pH of the sample needs to be less than the pK_a of the matrix for positive ion mass spectra [60], but beyond that studies probing the pH effect have varied widely depending on the matrix, analyte, and deposition conditions. During crystallization, evaporation of volatile species and precipitation can shift the reaction equilibrium, altering the charge species distribution and affecting the crystallization. These

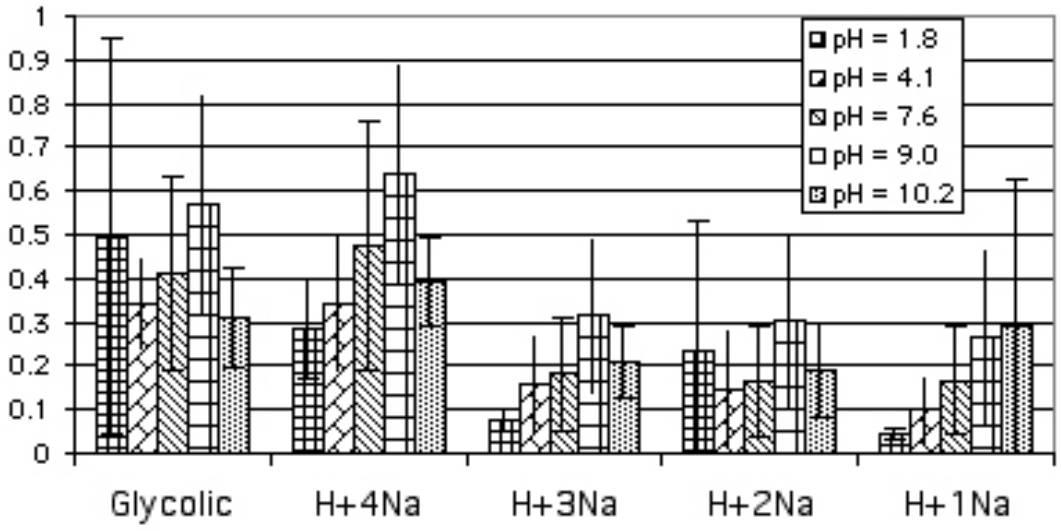

Figure 4.10. Normalized peak intensities from an equimolar mixture of glycolic acid and HEDTA in $NaNO_3$ at pH values ranging from 1.8 to 10.2. The five data sets represent glycolic acid and four HEDTA peaks of various degrees of adduction. (For example, "H+4Na" refers to an HEDTA ion with 4 sodium atoms - a sodium cation of the trisodium salt.)

factors, in addition to the bond formations intrinsic to the crystallization process and the incorporation of residual solvent, make it difficult to characterize the condensed phase charge associations based on the original solution pH.

However, several studies have observed that the initial charge states predicted by acid-base chemistry correspond to the ions observed in the mass spectra, suggesting that the preformed ions contribute significantly to the final ion yield. One such study mentioned above used indicators and found that the colors of the indicators are roughly preserved during crystallization and that the mass spectra qualitatively reflect the predicted solution species [20]. These results, in accordance with other studies [15,47], show a definite pH dependence, *i.e.* at lower solution pH values stronger (protonated) analyte ions are observed, while with increasing pH, and thus analyte deprotonation, the intensity of the protonated peaks in the mass spectra decrease while cation and cluster peaks increase. Residual solvent incorporated during crystallization was observed and assumed to aid in screening of counterions, potentially assisting in the separation of charges and survival of ions during cluster evaporation. However, one study of selected carboxylic compounds using a traditional MALDI matrix (2,5-DHB) and an

ultraviolet laser surprisingly showed an increase in ion yield for both the positive and negative ions with increasing pH [8].

One significant difference in the sodium nitrate studies compared to the studies described above is the identity of the charge carrying species. In the experiments described above divalent metal ions and protons were the source of charge, while in these studies sodium ions provided the source of positive charge. Hydrogen atoms, with a smaller atomic radius, can form shorter bonds, and thus stronger coulombic attractions. Accordingly, the stability constants, which represent the logarithm of the metal-ligand complex rate constant in solution, are a factor of 5-7 larger for hydrogen than sodium for polycarboxylic acids. While the larger atomic radius of sodium may result in more stable bidentate conformations as described in Section 4.3, it is unlikely that this alone will result in lower energy conformations than a (monodentate) hydrogen bond. Thus, a study on the effect of solution pH when sodium ions provide the primary source of charge is unlikely to show the same dependence as studies involving protons, as positively charged cations are unlikely to exist in the solution phase, but likely form instead either during crystallization or in the phase transition following laser irradiation.

Any signature of an effect due to the initial solution pH would instead appear in the distribution of the number of sodium atoms associated with analyte. At pH values below the (first) pK_a of the compound, the molecules are likely to be incorporated in their acid form, while at higher pH values, above the respective equivalence points, the deprotonated molecules will crystallize as salts. Assuming that this initial distribution is not altered by crystallization, then one might expect to see the degree of sodiation increase with pH. However, as seen in Figure 4.10, there is no such trend in the distribution of HEDTA salt peaks across the entire pH range, which almost completely spans the 3 equivalence points. If the pH changed significantly during evaporation, *e.g.* by evaporation of nitric acid, then one might expect that the precipitation would result in a sample with layers reflecting varying degrees of salting. However, irradiation of single spot of the sodium nitrate samples for several hundred laser shots did not reveal a shift in the sodium number distribution (data not shown), suggesting that differences in the composition of the sample due to precipitation rates are not significant.

Another difference in these sodium nitrate studies from more conventional MALDI systems is the low molecular weights of the‘analytes’ used here, which are comparable to that of the matrix, and raises questions as to whether the matrix truly performs the conventional MALDI

roles of isolating the analyte molecules and incorporating them into their crystalline structure. To test this possibility, single crystals of sodium nitrate were grown in solutions with carboxylic acids, and analyte ions were indeed detected from the surfaces of freshly cleaved faces. Also, the intensity of analyte ions was often unchanged after up to over a hundred laser shots from standard multicrystalline preparations, suggesting that the analyte ions do not reside solely on the surface, but are distributed uniformly throughout the sample.

A sample trisodium salt of HEDTA was added to sodium nitrate at an equivalent molar ratio to a HEDTA study, but no HEDTA ions were observed when irradiated at 7.1 μm. One might have expected to see results similar to HEDTA at high pH, where the fully deprotonated oxyanion most likely crystallizes as a trisodium salt. However, based on this observation, it appears that incorporation of the two species into the condensed phase results in different bonding arrangements that become important in the evolution to possible ion formation.

The studies considering the role of the initial pH of the sample, excepting the unexplained results for oxalic acid and the [HEDTA)Na^+ ion, indicate that the initial pH does not play a determining role in the final outcome of the ions. From a practical standpoint, this is encouraging for efforts to develop protocols for the mass spectrometric analysis of systems with a high salt content. When considering the mechanistic aspect of ion formation, these results seem to minimize the importance of the state of the ion in the solution phase in the case of weak binding, as molecules with different initial states result in similar ion profiles.

4.4. Summary

Mass spectrometry was successfully applied to the study of organic molecules in sodium nitrate using resonant vibrational excitation of the sodium nitrate, representing a new approach for the analysis of composite systems. The system studied here has significant differences from systems used in conventional MALDI experiments, and it remains to be seen how effective tunable infrared excitation of intrinsic matrices will be for the analysis of larger molecular weight compounds and systems without a high salt content. However, this study does show the benefits of excitation of modes with high optical absorption cross-sections, and that the absorption cross-section determines the particular mechanism of ablation and the final ion outcome. While it is known that sub-micron penetration depths are not required for successful

IR-MALDI, it does suggest that new candidate matrices should be screened, or even sought out, based on their optical properties. However, 'efficient' ablation by a high density of excitation is not sufficient (or even necessary) for successful IR-MALDI. Also, a suitable ionizing agent is required, unless secondary techniques like electron impact ionization or a secondary post-ionizing laser are employed. While sodium was a convenient and effective source for these studies, it was pointed out above that sodium often has deleterious consequences for many compounds. A small peptide (FMRF, M.W. ~600) was identified from sodium nitrate, although no further work was done to identify other compounds that might be detected from sodium nitrate. As noted in the introduction to this chapter, water has been shown to function as an effective matrix, even waters of hydration, and work in our lab is continuing to investigate these possibilities.

While the high salt content understandably results in the adduction of sodium molecules and ions, the number of sodium atoms present per molecule was observed to depend critically on the ablation pathway and molecular structure, but not on the initial solution charge state of the molecule. When sodium affinities of the carboxylic salts become available, the observed adduct distributions can be compared to reaction kinetics, allowing us to determine whether the ions are formed in thermodynamic equilibrium and further validating the results suggesting cationization occurring in the gas phase. Furthermore, sodium-binding affinities may quantitatively establish why protonation of salted carboxyl groups is not allowed, as evidenced by the need for alkali exchange for some biomolecules prior to analysis. The insights gleaned into the formation of carboxylic salts should be useful for those studying the importance of alkali metal-ligand associations in a variety of physical systems.

BIBLIOGRAPHY

[1] S. Berkenkamp, F. Kirpekar, and F. Hillenkamp, Science **281** (5374), 260 (1998).

[2] Stefan Berkenkamp, Christoph Menzel, Franz Hillenkamp, and Klaus Dreisewerd, Journal of the American Society for Mass Spectrometry **13** (3), 209 (2002).

[3] C. Menzel, S. Berkenkamp, and F. Hillenkamp, Rapid Communications in Mass Spectrometry **13** (1), 26 (1999).

[4] M. L. Baltz-Knorr, K. E. Schriver, and Jr. Haglund, R. F., Applied Surface Science **197-198**, 11 (2002).

[5] S. Berkenkamp, M. Karas, and F. Hillenkamp, Proceedings of the National Academy of Sciences of the United States of America **93** (14), 7003 (1996).

[6] M. Baltz-Knorr, D. R. Ermer, K. E. Schriver, and R. F. Haglund, Journal of Mass Spectrometry **37** (3), 254 (2002).

[7] J. E. Meacham, A. B. Webb, M. G. Plys et al., Safety Criteria for the Organic Watch List Tanks at the Hanford Site Report, Number, Westinghouse Hanford Company 1996.

[8] Steven C. Goheen, Karen L. Wahl, James A. Campbell, and Wayne P. Hess, J. Mass Spectrom. **32** (8), 820 (1997).

[9] Wayne P. Hess, Hee K. Park, Oguz Yavas, and R. F. Haglund Jr., Applied Surface Science **127-129**, 235 (1998).

[10] M. R. Papantonakis, D. R. Ermer, and R. F. Haglund Jr., Applied Surface Science **197-198**, 213 (2002).

[11] R. F. Haglund, M. Baltz-Knorr, D. R. Ermer, M. R. Papantonakis, and K. E. Schriver, Spectrochim. Acta, *Submitted* (2003).

[12] Michel W. F. Nielen, Mass Spectrometry Reviews **18** (5), 309 (1999).

[13] David J. Harvey, Mass Spectrometry Reviews **18** (6), 349 (1999).

[14] M. Karas, A. Ingendoh, U. Bahr, and F. Hillenkamp, Biomed. Environ. Mass Spectrom. **18** (9), 841 (1989).

[15] F. Dubois, R. Knochenmuss, Rjjm Steenvoorden, K. Breuker, and R. Zenobi, European Mass Spectrometry **2** (2-3), 167 (1996).

[16] W. Z. Zhang, S. F. Niu, and B. T. Chait, Journal of the American Society for Mass Spectrometry **9** (9), 879 (1998).

[17] Renato Zenobi and Richard Knochenmuss, Mass Spectrometry Reviews **17**, 337 (1998).

[18] Michael Karas, Matthias Gluckmann, and Jurgen Schafer, J. Mass Spectrom. **35** (1), 1 (2000).

[19] M. Karas and R. Kruger, Chemical Reviews **103** (2), 427 (2003).

[20] R Krüger, A Pfenninger, I Fournier, M Gluckmann, and M Karas, Analytical Chemistry **73** (24), 5812 (2001).

[21] Ralf Kruger and Michael Karas, Journal of the American Society for Mass Spectrometry **13** (10), 1218 (2002).

[22] Michael Karas, Ute Bahr, Isabelle Fournier, Matthias Gluckmann, and Anja Pfenninger, International Journal of Mass Spectrometry **226** (1), 239 (2003).

[23] L. V. Zhigilei, P. B. S. Kodali, and B. J. Garrison, Chemical Physics Letters **276** (3-4), 269 (1997).

[24] M. Gluckmann and M. Karas, Journal of Mass Spectrometry **34** (5), 467 (1999).

[25] A. Verentchikov, I. Smirnov, and M.L. Vestal, *47th ASMS Conference on Mass Spectrometry and Allied Topics*, Dallas, TX, June 13-17, 1999.

[26] A. N. Krutchinsky and B. T. Chait, Journal of the American Society for Mass Spectrometry **13** (2), 129 (2002).

[27] B. Spengler, M. Karas, U. Bahr, and F. Hillenkamp, Journal of Physical Chemistry **91** (26), 6502 (1987).

[28] Robert J. Cotter, Analytica Chimica Acta **195**, 45 (1987).

[29] H. Ehring, C. Costa, P. A. Demirev, and B. U. R. Sundqvist, Rapid Communications in Mass Spectrometry **10** (7), 821 (1996).

[30] R. Cramer, R. F. Haglund, and F. Hillenkamp, International Journal of Mass Spectrometry **169/170**, 51 (1997).

[31] J. Kampmeier, K. Dreisewerd, M. Schurenberg, and K. Strupat, International Journal of Mass Spectrometry **169/170**, 31 (1997).

[32] Bernhard Spengler and Dieter Kirsch, International Journal of Mass Spectrometry **226** (1), 71 (2003).

[33] R. Knochenmuss, A. Stortelder, K. Breuker, and R. Zenobi, Journal of Mass Spectrometry **35** (11), 1237 (2000).

[34] K. Breuker, R. Knochenmuss, J. Zhang, A. Stortelder, and R. Zenobi, International Journal of Mass Spectrometry **226** (1), 211 (2003).

[35] R. Knochenmuss and R. Zenobi, Chemical Reviews **103** (2), 441 (2003).

[36] T. D. McCarley, R. L. McCarley, and P. A. Limbach, Analytical Chemistry **70** (20), 4376 (1998).

[37] T. W. D. Chan, A. W. Colburn, and P. J. Derrick, Organic Mass Spectrometry **26** (4), 342 (1991).

[38] R. Knochenmuss, F. Dubois, M. J. Dale, and R. Zenobi, Rapid Communications in Mass Spectrometry **10** (8), 871 (1996).

[39] Richard Knochenmuss, Volker Karbach, Ursula Wiesli, Kathrin Breuker, and Renato Zenobi, Rapid Communications in Mass Spectrometry **12** (9), 529 (1998).

[40] M. E. Belov, C. P. Myatt, and P. J. Derrick, Chemical Physics Letters **284** (5-6), 412 (1998).

[41] Pao-Chi Liao and John Allison, Journal of Mass Spectrometry **30** (3), 408 (1995).

[42] Juan Zhang, Tae-Kyu Ha, Richard Knochenmuss, and Renato Zenobi, Journal of Physical Chemistry A **106** (28), 6610 (2002).

[43] Gilles Ohanessian, International Journal of Mass Spectrometry **219** (3), 577 (2002).

[44] J. Zhang, R. Knochenmuss, E. Stevenson, and R. Zenobi, International Journal of Mass Spectrometry **213** (2-3), 237 (2002).

[45] Juan Zhang, Vladimir Frankevich, Richard Knochenmuss, Sebastian D. Friess, and Renato Zenobi, Journal of the American Society for Mass Spectrometry **14** (1), 42 (2003).

[46] R. W. Nelson and T. W. Hutchens, Rapid Communications in Mass Spectrometry **6** (1), 4 (1992).

[47] Edda Lehmann, Richard Knochenmuss, and Renato Zenobi, Rapid Communications in Mass Spectrometry **11** (14), 1483 (1997).

[48] A. K. Sharma, S. A. Clauss, G. M. Mong, K. L. Wahl, and J. A. Campbell, J. Chromatogr., A **805**, 101 (1998).

[49] Helene Lavanant and Catherine Lange, Rapid Communications in Mass Spectrometry **16** (20), 1928 (2002).

[50] K. Dreisewerd, Chemical Reviews **103** (2), 395 (2003).

[51] O. Yavas, E. L. Maddocks, M. R. Papantonakis, and R. F. Haglund, Jr., Applied Surface Science **127-129**, 26 (1998).

[52] H. K. Park and R. F. Haglund, Applied Physics A-Materials Science & Processing **64** (5), 431 (1997).

[53] Lubert Stryer, *Biochemistry*, 4th ed. (W. H. Freeman, New York, 1995).

[54] John S. Klassen, Stephen G. Anderson, and Arthur T. Blades, The Journal of Physical Chemistry **100**, 14218 (1996).

[55] D A Griffith and A M Pajor, Biochemistry **38** (23), 7524 (1999).

[56] B. C. Guo, B. J. Conklin, and A. Welford Castleman, Jr., J. Am. Chem. Soc. **111** (17), 6506 (1989).

[57] J. M. Talley, B. A. Cerda, G. Ohanessian, and C. Wesdemiotis, Chemistry-A European Journal **8** (6), 1377 (2002).

[58] F. Jensen, Journal of the American Chemical Society **114** (24), 9533 (1992).

[59] B. A. Cerda, S. Hoyau, G. Ohanessian, and C. Wesdemiotis, Journal of the American Chemical Society **120** (10), 2437 (1998).

[60] H. Ehring, M. Karas, and F. Hillenkamp, Org. Mass Spectrom. **27** (4), 472 (1992).